

See discussions, stats, and author profiles for this publication at: <https://www.researchgate.net/publication/235421262>

# Controllable Adhesive Superhydrophobic Surfaces Based on PDMS Microwell Arrays

ARTICLE *in* LANGMUIR · FEBRUARY 2013

Impact Factor: 4.46 · DOI: 10.1021/la304492c · Source: PubMed

---

CITATIONS

37

READS

101

## 9 AUTHORS, INCLUDING:



Feng Chen

Xi'an Jiaotong University

155 PUBLICATIONS 1,274 CITATIONS

[SEE PROFILE](#)



Yang Qing

Xi'an Jiaotong University

80 PUBLICATIONS 576 CITATIONS

[SEE PROFILE](#)



Jinhai Si

Xi'an Jiaotong University

201 PUBLICATIONS 1,870 CITATIONS

[SEE PROFILE](#)



Xun Hou

Xi'an Jiaotong University

327 PUBLICATIONS 1,700 CITATIONS

[SEE PROFILE](#)

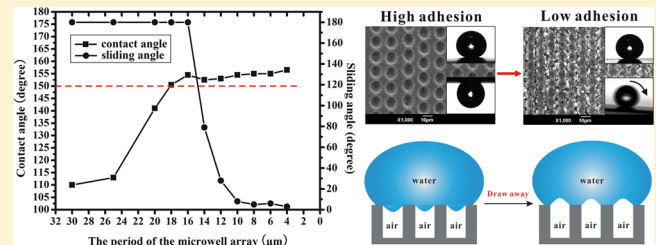
## Controllable Adhesive Superhydrophobic Surfaces Based on PDMS Micowell Arrays

Jiale Yong, Feng Chen,\* Qing Yang,\* Dongshi Zhang, Hao Bian, Guangqing Du, Jinhai Si, Xiangwei Meng, and Xun Hou

State Key Laboratory for Manufacturing System Engineering & Key Laboratory of Photonics Technology for Information of Shaanxi Province, School of Electronics & Information Engineering, Xi'an Jiaotong University, Xi'an, 710049, P. R. China

### Supporting Information

**ABSTRACT:** This paper presents a one-step method to fabricate superhydrophobic surfaces with extremely controllable adhesion based on PDMS micowell arrays. The micowell array structures are rapidly produced on PDMS films by a point-by-point femtosecond laser scanning process. The as-prepared superhydrophobic surfaces show water controllable adhesion that ranges from ultrahigh to ultralow by adjusting the extent of overlap of the adjacent micowell, on which the sliding angle can be controlled from 180° (a water droplet can not slide down even when the as-prepared surface is turned upside down) to 3°. A “micro-airbag effect” is introduced to explain the adhesion transition phenomenon of the micowell array structures. This work provides a facile and promising strategy to fabricate superhydrophobic surfaces with controllable adhesion.



### 1. INTRODUCTION

In nature, lotus leaves, duck feathers, moth compound eyes, water strider feet, and cicada wings exhibit the unusual phenomenon of superhydrophobicity, i.e., water contact angles (CAs) are above 150°.<sup>1–7</sup> Those surfaces usually have binary structures on the micro/nanoscale, resulting in high CAs and low drop sliding angles (SAs) smaller than 10°.<sup>8–11</sup> On the contrary, ultrahigh adhesion superhydrophobic surfaces like rose petals have recently been reported.<sup>12–16</sup> Though the CAs of water droplets are above 150° on such surfaces, the water droplets will not roll off even with the surfaces upside down. In recent years, a wide range of controllable adhesive superhydrophobic surfaces have attracted tremendous scientific interest due to their important applications in many fields, such as biochemical separation, transport of microdroplets, tissue engineering, and microfluidic chips.<sup>13,17–23</sup>

Generally, water adhesion on a superhydrophobic surface is mainly governed by the surface geometrical structure and chemical composition.<sup>24–26</sup> Therefore, through dynamically tuning the two factors, the water adhesion could be effectively controlled. For instance, Jiang et al. prepared a superhydrophobic aligned polystyrene nanotube layer, and obtained a controllable transition between high adhesive pinning and low adhesive rolling states.<sup>27,28</sup> Liu et al. reported a superhydrophobic MnO<sub>2</sub> nanostructured film with controllable adhesion by fabricating different patterns of MnO<sub>2</sub> nanocrystallites.<sup>17</sup> Xu et al. prepared a superhydrophobic cauliflower-like morphology by introduction of organic groups in silica nanospheres, and the adhesion could be modulated by adjusting the phenyl group content.<sup>29</sup> However, most reported methods used to fabricate superhydrophobic surfaces with

controllable adhesion generally require high-cost, complex fabrication processes and have tight restrictions on materials. More versatile and simple ways to fabricate superhydrophobic surfaces with controllable adhesion are still lacking.

Recently, micromachining for fabricating superhydrophobic surfaces by a femtosecond laser has attracted much interest because it is a simple method to realize three-dimensional (3D) structures with micro- and nanoscale hierarchic roughness, and it can be applied to a wide variety of materials.<sup>30–36</sup> In combination with a computer numerical control system, complex structures can be realized, which can exhibit unique wetting properties.<sup>21,23,31,36</sup> Here, we demonstrate a facile method to fabricate micowell array structured superhydrophobic PDMS surfaces with extremely controllable adhesion by a femtosecond laser. The surface microstructure could be controlled via adjusting the period of the micowell array which is generated by a point-by-point femtosecond laser scanning process. The CA and adhesion of the rough surfaces can be modulated by changing the surface morphology. The micowell array structured surfaces show superhydrophobicity, and the adhesion of these surfaces can be controlled from ultrahigh to ultralow by adjusting the extent of overlap of the adjacent micowell.

### 2. METHODS AND EXPERIMENTAL SECTION

PDMS is an elastomeric material, widely used in soft lithography and biomedicine. In the experiment, the PDMS thin films were generally

Received: August 30, 2012

Revised: February 2, 2013

Published: February 6, 2013



prepared from a 10:1 mixture (by weight) of prepolymer (DC-184A, Dow Corning Corporation) and curing agent (DC-184B, Dow Corning Corporation), poured onto the clean glass plate, and kept there for 10 min in a vacuum desiccator, so that the trapped air bubbles could emerge to the surface. After removing all the air bubbles, the mixture was solidified in an oven at 80 °C for 10 h. The solidified PDMS samples were carefully peeled off from the glass plate, and then rinsed with deionized water with sonication. The thickness of the PDMS samples was measured by a micrometer and was about 0.5 mm. Next, the PDMS samples were mounted on a motorized *x*-*y*-*z* translation stage controlled by computer and positioned perpendicularly to the direction of laser incidence, and then irradiated by a regenerative amplified Ti:sapphire laser system (Coherent, Libra-usp-1K-he-200) with a center wavelength of 800 nm which could afford 50 fs pulses at a repetition rate of 1 kHz, as shown in Figure 1a. The

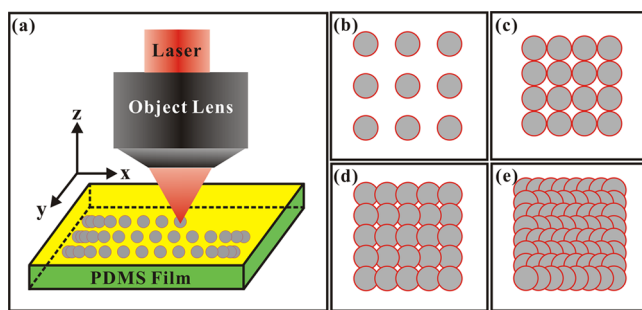


**Figure 1.** (a) Schematic illustration of the fabrication process. (b–e) Status of the as-prepared surfaces with different period of the microwell array: (b) separation, (c) tangency, (d) mild overlapping, and (e) strong overlapping.

Gaussian laser beam was focused by a microscope objective lens (10×, NA = 0.30, Nikon) on the front side of the sample with different laser power. A uniformly ablated crater with a rough bottom can be induced by a single laser pulse. The shape of the circular crater is similar to a microwell. The microwell array structures are rapidly generated on PDMS films by a point-by-point femtosecond laser scanning process. Following the irradiation process, the samples were cleaned by deionized water in an ultrasonic bath at room temperature for 10 min.

In the rapid scanning process, each single laser pulse can ablate a microwell. The surface morphology can be modulated by adjusting the period of the microwell array, which is denoted by the letter “*T*”. *T* is a

crucial machining parameter which is determined by the scanning speed and interval of adjacent laser scanning lines. Each scanning line consists of many transverse separated microwells. The transverse *T<sub>t</sub>* depends on the scanning speed because the laser system is a pulsed laser with a repetition rate of 1 kHz, and the lengthwise *T<sub>l</sub>* depends on the shift of adjacent laser scanning lines. In the experiment, we make *T<sub>t</sub>* approximately equal to *T<sub>l</sub>*, so that *T* ≈ *T<sub>t</sub>* ≈ *T<sub>l</sub>*. For example, *T* = 13 μm implies that the sample is fabricated at scanning speed of 13 000 μm/s and the interval of adjacent laser scanning lines is set at 13 μm. Here, we use four typical arrangements to simply show the status of the microwell array with different *T*, as shown in Figure 1b–e. With *T* decreasing, the adjacent microwells will change from “separation” to “tangency” to “mild overlapping”, and even to “strong overlapping”.

The morphology of the as-prepared surfaces irradiated by femtosecond laser pulses was characterized by a JSM-6390A scanning electron microscopy (JEOL, Japan). A LEXT-OLS4000 laser confocal microscope (Olympus, Japan) was also used to investigate the 2D images, 3D images, and cross-sectional profiles of the as-prepared surfaces. The water contact angles and the sliding angles of 8 μL water droplets on the surface were measured by an OCA20 contact-angle system (Dataphysics, Germany) at ambient temperature, using a sessile drop method.

### 3. RESULTS AND DISCUSSION

**Morphology of the Irradiated Surfaces.** Figure 2a–j show SEM images of the femtosecond laser irradiated PDMS surfaces with different *T* at a laser power of 30 mW and energy/pulse of 30 μJ. It is shown that a concave microwell with a diameter of 12.16 μm and a depth of 2.03 μm can be formed from a single laser pulse irradiation (Figure 2b and Figure 5a), and the microwell array structures are rapidly generated by a point-by-point femtosecond laser scanning process. With *T* decreasing, the microwells get close to each other and even overlap, similar to what is shown in Figure 1b–e. When *T* is equal to or greater than 16 μm, the microwells are nonoverlapping (Figure 2a,c). A uniformly ablated microwell with a rough bottom that is induced by a femtosecond laser pulse can be seen, and the outer region is randomly decorated with many nanoscale particles from the ejected material. The high-resolution SEM image of the nanoscale particles is shown in Supporting Information (Figure S1a). The adjacent microwells mildly overlap when *T* is between 14 and 12 μm

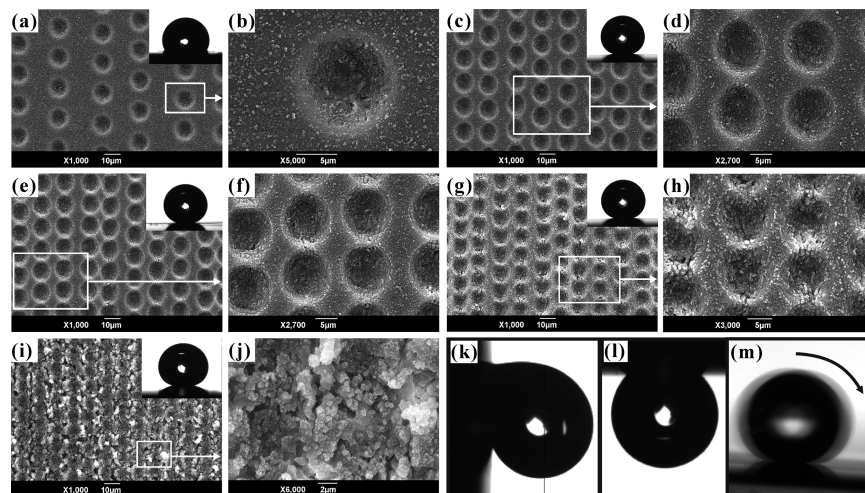


**Figure 2.** (a–j) Low- and high-magnification SEM images of the PDMS surfaces after femtosecond laser irradiation: (a,b) *T* = 25 μm; (c,d) *T* = 16 μm; (e,f) *T* = 14 μm; (g,h) *T* = 12 μm; (i,j) *T* = 10 μm. The insets show the shape of an 8 μL water droplet on the corresponding surfaces. (k,l) Shapes of a water droplet on the as-prepared surface with *T* = 16 μm tilted 90° and 180°, respectively. (m) A water droplet rolling on the 6° tilted as-prepared surface with *T* = 10 μm. The entire as-prepared surfaces are irradiated at a laser power of 30 mW.

(Figure 2f,h). The ripple formation is shown in the overlapping region (Supporting Information, Figure S1b). Therefore, a gap can be produced between the adjacent microwells. When  $T$  is equal to or smaller than  $10\ \mu\text{m}$ , the basic structure of the microwells will be destroyed and a new kind of rough surface will be formed due to the adjacent microwells with a strong overlap (Figure 2i,j). On such surfaces, many irregular nanoparticles with an average diameter of tens or hundreds of nanometers randomly distribute on the surface, some of which accumulated together to form one block like a water splash. Obviously, with  $T$  decreasing, the status of the as-prepared surface can be tuned from “separation” ( $T \geq 16\ \mu\text{m}$ ) to “mild overlapping” ( $10\ \mu\text{m} < T < 16\ \mu\text{m}$ ) to “strong overlapping” ( $T \leq 10\ \mu\text{m}$ ) when the as-prepared surfaces are irradiated at a laser power of  $30\ \text{mW}$ . This is consistent with what is shown in Figure 1b–e.

#### Wettability and Adhesion of the Irradiated Surfaces.

PDMS is a hydrophobic material with a water CA of  $110^\circ$  on the flat native layer. The water CA can be changed over a wide range from  $110^\circ$  to  $156.5^\circ$  when the PDMS surface is irradiated by femtosecond laser with different  $T$  at a laser power of  $30\ \text{mW}$ . When  $T$  is equal to  $25\ \mu\text{m}$ , the shapes of water droplets on the as-prepared surface are similar to those on the flat PDMS surface and the water CA is  $113^\circ$ , as shown in the inset of Figure 2a. However, when  $T$  is no more than  $18\ \mu\text{m}$ , the as-prepared surfaces show superhydrophobicity with water CA being larger than  $150^\circ$ . For example, the insets of Figure 2c and i show the shapes of a water droplet on the as-prepared PDMS surfaces with a water CA of  $154^\circ$  ( $T = 16\ \mu\text{m}$ ) and  $154.5^\circ$  ( $T = 10\ \mu\text{m}$ ), respectively. The water adhesion, which is an important property of a solid surface, can be accurately assessed by the sliding behavior of a water droplet. Interestingly, the experimental results show that the water droplet does not slide even when the as-prepared surfaces are  $90^\circ$  tilted (Figure 2k) or turned upside down (Figure 2l) when  $T$  is greater than or equal to  $16\ \mu\text{m}$  (Supporting Information, Movie S1), but the water droplet can move very easily even when the surfaces are only slightly tilted (Figure 2m) or shaken when  $T$  is no more than  $10\ \mu\text{m}$  (Supporting Information, Movie S2). In order to evaluate the relationship between the period of the microwell array and the surface wettability and adhesion, PDMS surfaces irradiated with different  $T$  were selected and compared as shown in Figure 3.

The period of the microwell array, which is the most crucial structure parameter, has an important effect on the water CA and SA of the as-prepared surfaces. Figure 3a shows the relationships between  $T$  and the CA/SA, respectively (at a laser power of  $30\ \text{mW}$ ). It can be clearly seen that the CA originally increases with decreasing  $T$  and then stabilizes above  $150^\circ$ . On the other hand, with the decrease of  $T$ , SA remains at  $180^\circ$  (indicating that the water droplet does not slide down even when the as-prepared surface is turned upside down) and then sharply decreases from  $180^\circ$  ( $T = 16\ \mu\text{m}$ ) to  $6^\circ$  ( $T = 10\ \mu\text{m}$ ). In particular, the SA can be as low as  $3^\circ$  when  $T = 4\ \mu\text{m}$ . It is worth noting that all the CAs near the SA variable region are larger than  $150^\circ$ . This result implies that there is a transition between the superhydrophobic surface with ultrahigh adhesion and the superhydrophobic surface with ultralow adhesion for the PDMS surfaces irradiated by a femtosecond laser. The superhydrophobic surface with ultrahigh adhesion can be obtained with  $T$  between  $18$  and  $16\ \mu\text{m}$ . Conversely, the superhydrophobic surfaces with ultralow adhesion can be obtained in a wide range of  $T$  from  $10$  to  $4\ \mu\text{m}$ . In the range of

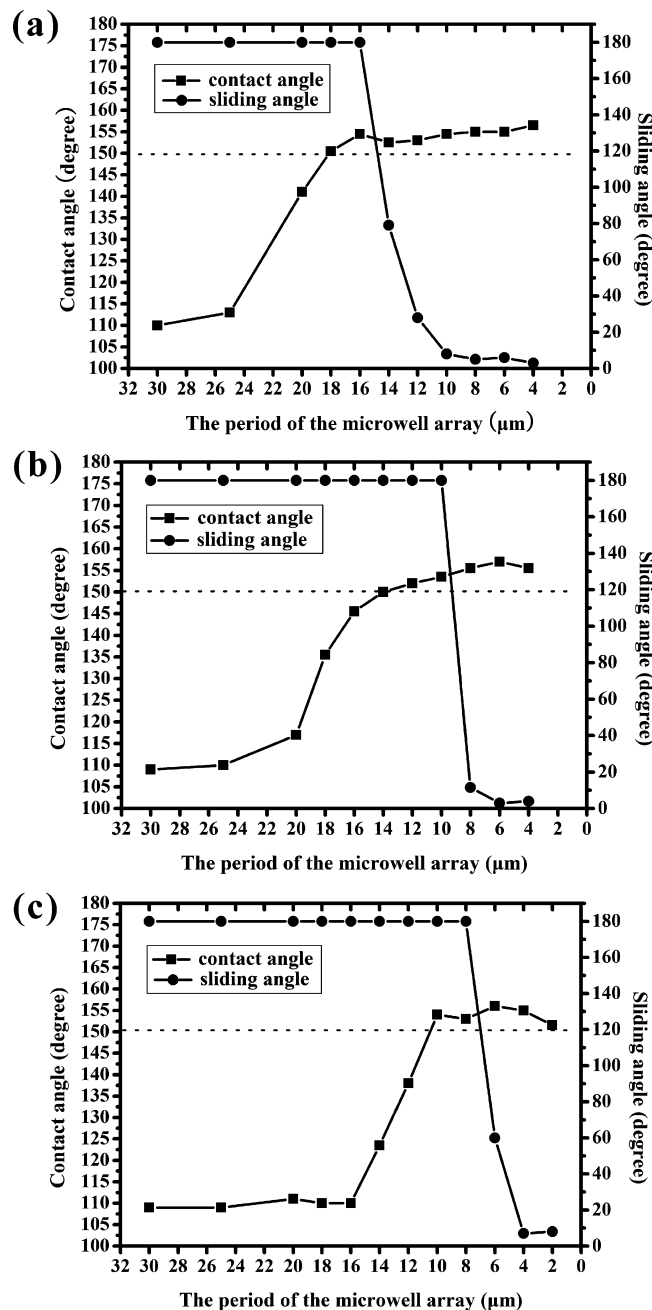


**Figure 3.** Relationships between the period of the microwell array ( $T$ ) and the CA (left)/SA (right), respectively. The as-prepared surfaces are irradiated at a laser power of (a)  $30\ \text{mW}$ , (b)  $20\ \text{mW}$ , and (c)  $10\ \text{mW}$ , respectively.

$T$  from  $16$  to  $10\ \mu\text{m}$ , the adhesion can be controlled from ultrahigh to ultralow. A similar phenomenon can also be observed in the case of laser power of  $20\ \text{mW}$  (Figure 3b) and laser power of  $10\ \text{mW}$  (Figure 3c). It is clear that the as-prepared superhydrophobic surfaces irradiated by femtosecond laser show controllable adhesion by adjusting the period of the microwell array.

**Potential Mechanism for the Superhydrophobicity and the Adhesion Transition.** The CA on a composite surface can be expressed by the Cassie–Baxter equation:<sup>37,38</sup>

$$\cos \theta_c = f \cos \theta + f - 1$$

where  $\theta_c$  and  $\theta$  are the CAs on a surface with rough and flat structures, respectively, and  $f$  is the fraction of the surface which is in contact with the liquid. It is easy to deduce from this equation that increasing the roughness of the surface will lead to an increase of  $\theta_c$  because the value of  $f$  is inversely related to the roughness of the surface. In our experiment, a microwell can be formed from a laser pulse. With  $T$  decreasing, the status of the microwell arrays will change from “separation” to “tangency” to “mild overlapping”, and even to “strong overlapping”, as shown in Figure 2a–j. Meanwhile, the density of the microwells increases gradually. On the other hand, the density of the nanoscale particles outside the microwell also increases as the  $T$  becomes smaller due to the cumulative effect. The microscale and nanoscale changes significantly increase the roughness of the as-prepared surface, which leads to the CA increasing from intrinsic  $110^\circ$  to an angle more than  $150^\circ$ . This result is consistent with Cassie–Baxter model. In particular, for the status of “strong overlapping”, the surface shows a uniform micro/nanocomposite roughness, and in this case, the microwell array structures completely disappear. The morphology of the as-prepared surfaces shows another kind of structure with uniform roughness, which is significantly different from the status of “separation” and “mild overlapping”. The micro/nanocomposite structure can trap a large amount of air, which is helpful to decrease the contact area between water and the solid surface and makes the CA higher than  $150^\circ$ .

The adhesion of the as-prepared surfaces shows a close relationship with the morphology of the surface. Especially, microwells play an important role in it. As shown in Figure 4,

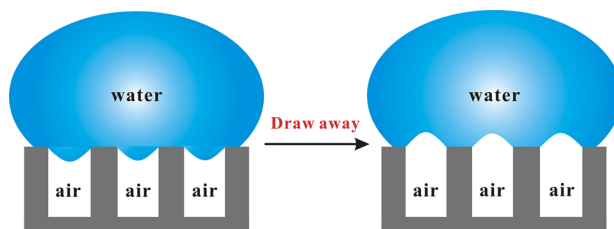


**Figure 4.** Schematic illustration of the “micro-airbag effect”. An airtight airbag is formed between the microwell and the liquid/air interface. When the water droplet is gradually drawn away from a microwell array, the meniscus on each microwell nozzle would change from concave to convex, leading to an increased volume of air in each airtight airbag. This expansion of air would result in the formation of a negative pressure which can greatly increase the adhesion of the surface.

the microwell generated by a single laser pulse irradiation and the liquid/air interface forms an airtight airbag. When a water droplet is gradually drawn away from the microwells upward, the meniscus on each microwell would be changed from concave to convex. This change can make an increased volume of air in each airtight airbag. According to Boyle’s law, the pressure has an inverse relationship with the volume for an ideal gas when the conditions of quality and temperature are constant.<sup>28,39</sup> Therefore, this expansion of air would result in the formation of a negative pressure which can greatly increase the adhesion of the as-prepared surfaces. Here, we call it “micro-airbag effect”.

For the status of “separation”, when  $T$  is large enough, the adjacent microwells generated by pulsed laser irradiation are so sparse that the adhesion comes mainly from the intrinsically high adhesion of PDMS for water. The effect of the microwells

is negligibly small. As  $T$  decreases, the contact area between water and the flat PDMS area also decreases because the water would not contact the inner surface of the microwells according to the Cassie/Baxter model, but the adhesion of the as-prepared surface should not diminish because the effect of the microwells becomes more prominent. The “micro-airbag effect” results in the SA remaining at  $180^\circ$  when the adjacent microwells are separate. However, when the adjacent microwells are in the status of “strong overlapping” (Figure 2j), the microwell structures are gravely damaged and will finally disappear. The surfaces show a uniform micro/nanocomposite rough morphology, and the microwells’ induced “micro-airbag effect” will disappear. In this case, the as-prepared surfaces show ultralow adhesion, similar to a lotus leaf.

The surfaces in the “separation” regime show hydrophobicity to superhydrophobicity with ultrahigh water adhesion, and the surfaces in the “strong overlapping” regime show superhydrophobicity with ultralow water adhesion. Between these extremes, the main status is “mild overlapping”. When the adjacent microwells mildly overlap (Figure 2f,h), part of the microwells will be damaged and the edges near the microwells become rougher. In addition, some gaps are produced between those adjacent microwells and the airtightness of the airbag is weakened. To a certain degree, the “micro-airbag effect” will also be weakened. The damage of the microwells has a positive relationship with the extent of overlap of the adjacent microwells. In this case, by simply adjusting the extent of overlap of the adjacent microwells, the adhesion of the superhydrophobic surfaces can be controlled from ultrahigh to ultralow, as shown in Figure 3.

It is revealed that the airtight airbag between the microwell formed by a laser pulse and the liquid/air interface can lead to ultrahigh adhesion, and the adhesion of the as-prepared surfaces can be controlled from ultrahigh to ultralow as the airtightness of the airbag is weakened by decreasing  $T$ . This conclusion is also verified in the case of laser power of 20 mW (Figure 3b) and laser power of 10 mW (Figure 3c). The critical range of  $T$  for the adhesion transition is  $16\text{--}10 \mu\text{m}$  (30 mW),  $10\text{--}6 \mu\text{m}$  (20 mW), and  $8\text{--}4 \mu\text{m}$  (10 mW), respectively, which gradually decreases with smaller laser power. This trend is consistent with the diameter change of the microwells of the as-prepared surfaces, as shown in Figure 5. The diameter of a microwell irradiated by a single laser pulse at the laser power of 30 mW, 20 mW, and 10 mW is  $12.16 \mu\text{m}$ ,  $8.68 \mu\text{m}$ , and  $5.08 \mu\text{m}$ , respectively. The diameter of the microwell irradiated at laser power of 10 mW is smaller than at laser power of 30 mW, so the microwell array needs a smaller period ( $T$ ) for the adjacent microwells to be mildly overlapping. This consistency of the critical range of  $T$  for the adhesion transition and the diameter of the microwells at different laser power shows that the microairbag effect is valid.

#### 4. CONCLUSIONS

In conclusion, we report a one-step method to fabricate superhydrophobic surfaces based on PDMS microwell arrays by a femtosecond laser. Comparing with a traditional superhydrophobic surface, the adhesion of the surfaces can be controlled from ultrahigh to ultralow by adjusting the period of the microwell arrays ( $T$ ). It reveals that the airtight airbag in the microwell and covered by the liquid/air interface can lead to ultrahigh adhesion, and the adhesion of the as-prepared surfaces can be changed from ultrahigh to ultralow as the airtightness of the airbag is weakened by decreasing  $T$ . We believe that the

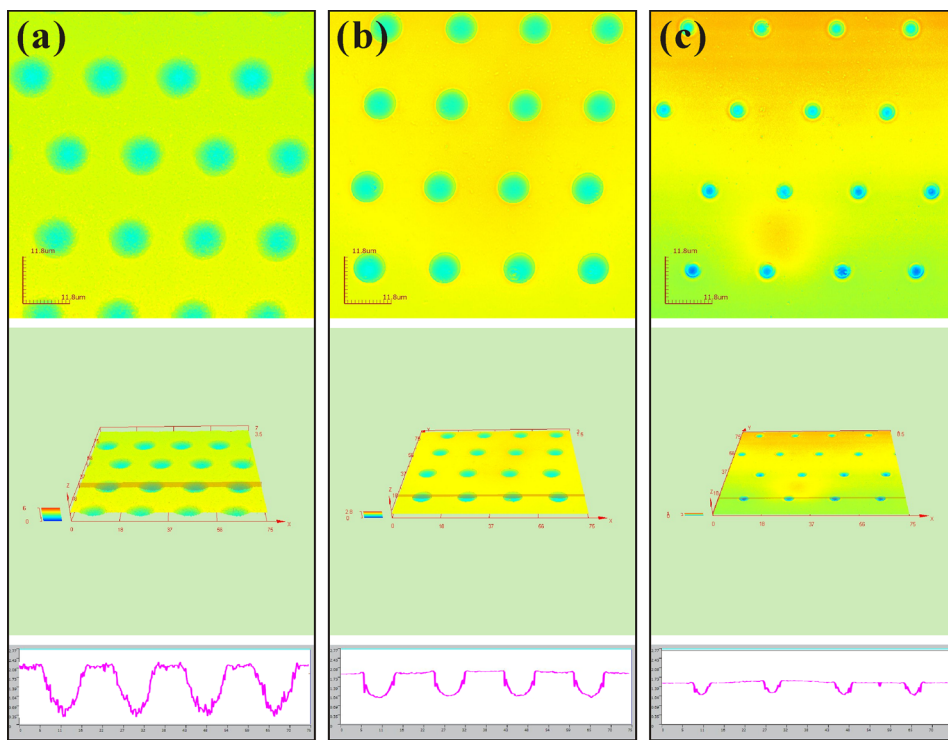


**Figure 5.** 2D images, 3D images, and cross-sectional profiles of the as-prepared surfaces: (a) laser power = 30 mW; (b) laser power = 20 mW; (c) laser power 10 mW. All the samples were fabricated with  $T = 20 \mu\text{m}$  and were magnified 3400 $\times$ .

approach developed to control the adhesion of the superhydrophobic surfaces by this simple method will have important potential applications in the manipulation of water droplets/fluid.

## ■ ASSOCIATED CONTENT

### Supporting Information

Figure S1; Movies S1 and S2. This material is available free of charge via the Internet at <http://pubs.acs.org>.

## ■ AUTHOR INFORMATION

### Corresponding Author

\*E-mail addresses: chenfeng@mail.xjtu.edu.cn; yangqing@mail.xjtu.edu.cn.

### Notes

The authors declare no competing financial interest.

## ■ ACKNOWLEDGMENTS

This work is supported by the National Science Foundation of China under the Grant nos. 61176113, National High Technology R&D Program of China under the Grant no. 2009AA04Z305 and the Fundamental Research Funds for the Central Universities.

## ■ REFERENCES

- (1) Genzel, J.; Efimenko, K. Recent Development in Superhydrophobic Surfaces and Their Relevance to Marine Fouling: a Review. *Biofouling* **2006**, *22*, 339–360.
- (2) Gao, X. F.; Jiang, L. Water-Repellent Legs of Water Striders. *Nature* **2004**, *432*, 36.
- (3) Liu, K.; Jiang, L. Bio-Inspired Self-Cleaning Surfaces. *Annu. Rev. Mater. Res.* **2012**, *42*, 231–263.
- (4) Li, X. M.; Reinhoudt, D.; Crego-Calama, M. What Do We Need for a Superhydrophobic Surface? A Review on the Recent Progress in the Preparation of Superhydrophobic Surfaces. *Chem. Sov. Rev.* **2007**, *36*, 1350–1368.
- (5) Bhushan, B. Biomimetics: Lessons from Nature – an Overview. *Philos. Trans. R. Soc. A* **2009**, *367*, 1445–1486.
- (6) Yao, X.; Song, Y. L.; Jiang, L. Applications of Bio-Inspired Special Wettable Surfaces. *Adv. Mater.* **2011**, *23*, 719–734.
- (7) Liu, K. S.; Jiang, L. Bio-Inspired Design of Multiscale Structures for Function Integration. *Nano Today* **2011**, *6*, 155–175.
- (8) Xia, F.; Jiang, L. Bio-Inspired, Smart, Multiscale Interfacial Materials. *Adv. Mater.* **2008**, *20*, 2842–2858.
- (9) Barthlott, W.; Neinhuis, C. Purity of the Sacred Lotus, or Escape from Contamination in Biological Surfaces. *Planta* **1997**, *202*, 1–8.
- (10) Zhang, X.; Shi, F.; Niu, J.; Jiang, Y. G.; Wang, Z. Q. Superhydrophobic Surfaces: from Structural Control to Functional Application. *J. Mater. Chem.* **2008**, *18*, 621–633.
- (11) Feng, L.; Zhang, Y.; Xi, J. M.; Wang, N.; Xia, F.; Jiang, L. Petal Effect: a Superhydrophobic State with High Adhesive Force. *Langmuir* **2008**, *24*, 4114–4119.
- (12) Lee, H.; Lee, B. P.; Messersmith, P. B. A Reversible Wet/Dry Adhesive Inspired by Mussels and Geckos. *Nature* **2007**, *448*, 338–342.
- (13) Liu, X. J.; Liang, Y. M.; Zhou, F.; Liu, W. M. Extreme Wettability and Tunable Adhesion: Biomimicking beyond Nature? *Soft Matter* **2012**, *8*, 2070–2086.
- (14) Zheng, Y. M.; Gao, X. F.; Jiang, L. Directional Adhesion of Superhydrophobic Butterfly Wings. *Soft Matter* **2007**, *3*, 178–182.
- (15) Parker, A. R.; Lawrence, C. R. Water Capture by a Desert Beetle. *Nature* **2001**, *414*, 33–34.
- (16) Zhai, L.; Berg, M. C.; Cebeci, F. C.; Kim, Y.; Milwid, J. M.; Rubner, M. F.; Cohen, R. E. Patterned Superhydrophobic Surfaces: Toward a Synthetic Mimic of the Namib Desert Beetle. *Nano Lett.* **2006**, *6*, 1213–1217.
- (17) Zhou, X. D.; Fan, H. M.; Liu, X. Y.; Pan, H. H.; Xu, H. Y. Pattern-Dependent Tunable Adhesion of Superhydrophobic MnO<sub>2</sub> Nanostructured Film. *Langmuir* **2011**, *27*, 3224–3228.
- (18) Sun, T. L.; Qing, G. Y. Biomimetic Smart Interface Materials for Biological Applications. *Adv. Mater.* **2011**, *23*, H57–H77.

- (19) Liu, M. J.; Jiang, L. Switchable Adhesion on Liquid/Solid Interfaces. *Adv. Funct. Mater.* **2010**, *20*, 3753–3764.
- (20) Wu, D.; Wu, S. Z.; Chen, Q. D.; Zhang, Y. L.; Yao, J.; Niu, L. G.; Wang, J. N.; Jiang, L.; Sun, H. B. Curvature-Driven Reversible In Situ Switching Between Pinned and Roll-Down Superhydrophobic States for Water Droplet Transportation. *Adv. Mater.* **2011**, *23*, 545–549.
- (21) Chen, F.; Zhang, D. S.; Yang, Q.; Wang, X. H.; Dai, B. J.; Li, X. M.; Hao, X. Q.; Ding, Y. H.; Si, J. H.; Hou, X. Anisotropic Wetting on Microstrips Surface Fabricated by Femtosecond Laser. *Langmuir* **2011**, *27*, 359–365.
- (22) Shirtcliffe, N. J.; McHale, G.; Newton, M. I. Learning from Superhydrophobic Plants: The Use of Hydrophilic Areas on Superhydrophobic Surfaces for Droplet Control. *Langmuir* **2009**, *25*, 14121–14128.
- (23) Zhang, D. S.; Chen, F.; Yang, Q.; Yong, J. L.; Bian, H.; Ou, Y.; Si, J. H.; Meng, X. W.; Hou, X. A Simple Way to Achieve Pattern-Dependent Tunable Adhesion in Superhydrophobic Surfaces by a Femtosecond Laser. *ACS Appl. Mater. Interfaces* **2012**, *4*, 4905–4912.
- (24) Li, J.; Liu, X. H.; Ye, Y. P.; Zhou, H. D.; Chen, J. M. Fabrication of Superhydrophobic CuO Surfaces with Tunable Water Adhesion. *J. Phys. Chem. C* **2011**, *115*, 4726–4729.
- (25) Whyman, G.; Bormashenko, E. How to Make the Cassie Wetting State Stable? *Langmuir* **2011**, *27*, 8171–8176.
- (26) Wong, T. K.; Kang, S. H.; Tang, S. K. Y.; Smythe, E. J.; Hatton, B. D.; Grinthal, A.; Aizenberg, J. Bioinspired Self-Repairing Slippery Surfaces with Pressure-Stable Omniphoticity. *Nature* **2011**, *477*, 443–447.
- (27) Jin, M. H.; Feng, X. J.; Feng, L.; Sun, T. L.; Zhai, J.; Li, T. J.; Jiang, L. Superhydrophobic Aligned Polystyrene Nanotube Films with High Adhesive Force. *Adv. Mater.* **2005**, *17*, 1977–1981.
- (28) Lai, Y. K.; Gao, X. F.; Zhuang, H. F.; Huang, J. Y.; Lin, C. J.; Jiang, L. Designing Superhydrophobic Porous Nanostructures with Tunable Water Adhesion. *Adv. Mater.* **2009**, *21*, 3799–3803.
- (29) Wang, M.; Chen, C.; Ma, J. P.; Xu, J. Preparation of Superhydrophobic Cauliflower-like Silica Nanospheres with Tunable Water Adhesion. *J. Mater. Chem.* **2011**, *21*, 6962–6967.
- (30) He, S. G.; Chen, F.; Liu, K. Y.; Yang, Q.; Liu, H. W.; Bian, H.; Meng, X. W.; Shan, C.; Si, J. H.; Zhao, Y. L.; Hou, X. Fabrication of Three-Dimensional Helical Microchannels with Arbitrary Length and Uniform Diameter inside Fused Silica. *Opt. Lett.* **2012**, *37*, 3825–3827.
- (31) Zhang, D. S.; Chen, F.; Yang, Q.; Si, J. H.; Hou, X. Mutual Wetting Transition between Isotropic and Anisotropic on Directional Structures Fabricated by Femtosecond Laser. *Soft Matter* **2011**, *7*, 8337–8342.
- (32) Baldacchini, T.; Carey, J. E.; Zhou, M.; Mazur, E. Superhydrophobic Surfaces Prepared by Microstructuring of Silicon Using a Femtosecond Laser. *Langmuir* **2006**, *22*, 4917–4919.
- (33) Barberoglou, M.; Zorba, V.; Stratidakis, E.; Tzanetakis, P.; Anastasiadis, S. H.; Fotakis, C. Bio-Inspired Water Repellent Surfaces Produced by Ultrafast Laser Structuring of Silicon. *Appl. Surf. Sci.* **2009**, *255*, 5425–5429.
- (34) Bonse, J.; Bandach, S.; Kruger, J.; Kautek, W.; Lenzer, M. Femtosecond Laser Ablation of Silicon-Modification Thresholds and Morphology. *Appl. Phys. A: Mater. Sci. Process.* **2002**, *74*, 19–25.
- (35) Liu, H. W.; Chen, F.; Wang, X. H.; Yang, Q.; Bian, H.; Si, J. H.; Hou, X. Influence of Liquid Environments on Femtosecond Laser Ablation of Silicon. *Thin Solid Films* **2010**, *518*, 5188–5194.
- (36) Zhang, D. S.; Chen, F.; Fang, G. P.; Yang, Q.; Xie, D. G.; Qiao, G. J.; Li, W.; Si, J. H.; Hou, X. Wetting Characteristics on Hierarchical Structures Patterned by a Femtosecond Laser. *J. Micromech. Microeng.* **2010**, *20*, 075029.
- (37) Cassie, A. B. D.; Baxter, S. Wettability of Porous Surfaces. *Trans. Faraday Soc.* **1944**, *40*, 546–551.
- (38) Whyman, G.; Bormashenko, E.; Stein, T. The Rigorous Derivation of Young, Cassie-Baxter and Wenzel Equations and the Analysis of the Contact Angle Hysteresis Phenomenon. *Chem. Phys. Lett.* **2007**, *450*, 355–359.
- (39) West, J. B. The Original Presentation of Boyle's Law. *J. Appl. Physiol.* **1999**, *87*, 1543–1545.